Heliyon 10 (2024) e30368

Contents lists available at ScienceDirect

Heliyon

journal homepage: www.cell.com/heliyon

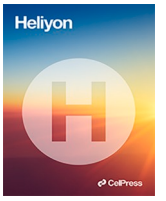

Research article

Evaluation of the CH_4/CO_2 separation by adsorption on coconut shell activated carbon: Impact of the gas moisture on equilibrium selectivity and adsorption capacity

Junior Staudt [a,*], Cassiano Moreira Musial [a], Rafael Canevesi [b], Vanessa Fierro [b], Caroline Ribeiro [a], Helton José Alves [c], Carlos Eduardo Borba [a]

[a] Postgraduate Program in Chemical Engineering, West Parana State University, Campus Toledo, Faculdade St. 645, Jd. La Salle, 85903-000, Toledo, PR, Brazil
[b] Institut Jean Lamour, CNRS, Université de Lorraine, no 7198, ENSTIB, 27 rue Philippe Séguin, BP 21042, 88051 Epinal Cedex 9, France
[c] Laboratory of Catalysis and Biofuel Production (LabCatProBio), Federal University of Parana (UFPR - Setor Palotina), Palotina, PR, Brazil

ARTICLE INFO

Keywords:
Biomethane
Water vapor
Experimental binary equilibrium
Simulated ternary equilibrium
Pressure swing adsorption

ABSTRACT

Upgrading biogas to biomethane is of great interest to change the energy matrix by feeding the renewable fuel produced from biomass waste into natural gas grids or directly using it to replace fossil fuels. The study aimed to assess the adsorption equilibrium of CH_4, CO_2, and H_2O on a coconut-shell activated carbon (CAC 8X30) to provide data for further studies on its efficiency in upgrading biogas by Pressure Swing Adsorption (PSA). The adsorbent was characterized, and equilibrium parameters were estimated from monocomponent CH_4, CO_2, and H_2O equilibrium isotherms. Binary and ternary equilibrium isotherms were simulated, and the selectivity and adsorption capacity of the CAC 8X30 were calculated in dry and wet conditions and then compared with zeolite 13X as a reference material. Regarding characterization, Nitrogen and Hydrogen Physisorption results indicated that 94 % of the pore volume is concentrated in the region of micropores. The adsorption affinity with CAC 8X30 estimated from monocomponent isotherms was in the order $K_{H20}>K_{CO2}>K_{CH4}$. IAST-Langmuir model simulations presented good agreement with experimental binary equilibrium data. Further simulations indicated equilibrium selectivity for CO_2 over CH_4 (e.g., 4.7 at 1 bar and 298 K for a mixture of CH_4/CO_2, 60/40 vol%), which increased in the presence of moisture, indicating its suitability for upgrading humid biogas. Simulations for zeolite 13X suggested that the material is unsuitable in the presence of water vapor but presents higher selectivity than the CAC 8X30 in dry conditions. Hence, the integration of both materials might be helpful for biogas upgrading.

1. Introduction

Biogas has been widely studied as an essential alternative for expanding the world's energy supply since it causes lower emissions of carbon dioxide, nitrogen oxides, and particulates compared to other fuels such as oil and coal [1,2]. However, the feasibility of applying biogas as a fuel depends on the removal of minor components such as water vapor (H_2O) and hydrogen sulfide (H_2S) (purification) and the removal of CO_2 from the main mixture of raw biogas formed by CH_4/CO_2 (upgrading) [3–5]. The fuel obtained after

* Corresponding author.
E-mail address: junior.staudt.js@gmail.com (J. Staudt).

https://doi.org/10.1016/j.heliyon.2024.e30368
Received 12 October 2023; Received in revised form 2 April 2024; Accepted 24 April 2024
Available online 30 April 2024

upgrading, namely biomethane, presents a high methane purity, whose exact value depends on local legislation. In general, biomethane must present a composition of methane of over 90 mol% ($CH_4 \geq 90$ mol%), whereas CO_2 cannot exceed 3 mol.% ($CO_2 \leq 3$ mol.%).

There are currently many known techniques for biogas purification and upgrading, including Membranes [6,7], Chemical Absorption and Water Scrubbing [8,9] and Adsorption [10,11]. Among these, Pressure Swing Adsorption (PSA) stands out because it provides high-purity methane and high automation capacity, and there are no chemical agents other than the adsorbent. On the other hand, the installation of PSA plants is often impaired by the high initial investment, driven by the high cost of commonly used commercial adsorbents, such as carbon molecular sieves, zeolites, and metal-organic frameworks [2,12]. In fact, the chosen material must present a low cost, in addition to technical aspects such as high equilibrium and kinetic selectivity, elevated CO_2 adsorption capacity, and easy regeneration [13].

In general, activated carbons (AC) represent costs up to 100 times lower per kilogram of material than other materials [14] and their potential for upgrading biogas has already been reported [15–17]. Besides that, the study of Durán and coworkers [17] using plant-origin activated carbon showed that the material was selective to CO_2 even in the presence of moisture, suggesting that the carbonaceous material might remove water vapor and provide the upgrading of biogas simultaneously, eliminating the need for an additional column. Vilella and coworkers [16] synthesized a coconut AC and evaluated it at low-pressure ranges regarding the separation of the mixture CH_4/CO_2. The material presented selectivity and working capacity values comparable to the tested commercial adsorbents.

The commercial coconut-shell activated carbon (CAC 8X30) used in this paper was successfully used to remove H_2S from raw biogas [18] and for methane storage [19]. To the best of our knowledge, however, there are no reports about its efficiency in upgrading biogas nor about the influence of moisture on the selectivity for CO_2. The present study aims to develop an experimental and theoretical assessment of the adsorption equilibrium of CH_4, CO_2, and H_2O on CAC 8X30 to provide data for further studies on its efficiency in upgrading biogas to biomethane by PSA. The AC was characterized by Physisorption, Helium Pycnometry, Mercury Porosimetry, Elemental Analysis, DSC, FTIR, and Raman. Monocomponent equilibrium data were obtained for the three components from adsorption isotherms at temperatures of 298 and 323 K, and binary equilibrium data (CH_4/CO_2) from breakthrough curves at 298 K. The predictions were evaluated by the Ideal Adsorbed Solution Theory (IAST), through parameters obtained from the monocomponent isotherms, fitted by Langmuir and Multisite Langmuir models, and through the respective extended models. Besides, the selectivity for CO_2 was simulated for binary (CH_4/CO_2) and ternary ($CH_4/CO_2/H_2O$) mixtures to assess biogas upgrading by the CAC 8X30 in the presence of moisture.

2. Material and methods

2.1. Materials

Coconut shell activated carbon (CAC 8X30) was supplied by the company Brascarbo Agroindustrial Ltda™. The gases used for the experiments (CO_2, CH_4, H_2O, and He) were of analytical grade, with purity $\geq$ 99.995 %.

Table 1
Physical and chemical characterization techniques and methodologies used in the present work.

Technique	Procedure
Physisorption	Textural properties were assessed following the methods described by Castro-Gutiérrez [20] and Jagiello [21] for heterogeneous surfaces. N_2 and H_2 isotherms were obtained using a 3FLEX (Micromeritics) adsorption apparatus. The pore size distributions (PSDs) and the surface area were calculated by combining N_2 and H_2 sorption data, and SAIEUS software was used to apply the two-dimensional nonlocal density functional theory (2D-NLDFT). By integration of the PSDs, total pore volumes (V_T), ultramicropore volume ($V_{ult\text{-}micro}$), supermicropore volume ($V_{sup\text{-}micro}$), micropore volume (V_{micro}), and mesopore volume (V_{mes}) were calculated. The PSDs were also used to calculate the average pore size (L_0) and average micropore size ($L_{0\text{-}micro}$).
Mercury Porosimetry	The material's porosity was assessed by Hg porosimetry on Auto Pore IV equipment (Micromeritics).
Helium Pycnometry	The analysis of Helium Pycnometry (AccuPyc 1330 – Micromeritics) was carried out to obtain the density of the material, using a rate of equilibration of 0.0050 psi min^{-1}, 20 purges and 10 runs at 19.5 psi.
Differential Scanning Calorimetry (DSC)	DSC run was conducted from 15 to 100 °C (DSC-60, Shimadzu) with a nitrogen flow rate of 20 ml min^{-1}. The heat capacity of the CAC 8X30 was then determined following the standard DIN 51007 [22,23].
Elemental Analysis	Bulk contents of C, H, N, S, and O were measured in a Vario EL Cube analyzer. Previously dried samples of 2 mg were placed in the equipment. The samples were combusted, and the generated gases were separated using selective adsorption. The content of combustion gases was analyzed using a thermal conductivity detector for C, H, N, and S. On the other hand, the oxygen content was measured based on the CO peak.
Fourier-Transform Infrared Spectroscopy (FTIR)	FTIR spectroscopy (Perkin Elmer) was used to assess the surface functional groups of pristine activated carbon (PAC) and used activated carbon (UAC). The UAC was submitted to several CH_4 and CO_2 adsorption/desorption cycles. The spectra were obtained by diffuse reflectance in the mid-infrared region, between 4000 and 450 cm^{-1}, with a resolution of 4 cm^{-1} and 16 accumulations.
Raman Spectroscopy	Horiba micro-Raman system, model LabRAM HR Evolution. Laser power 10 mW, 405 nm excitation wavelength, and CCD detector with additional sample preparation. Voigt functions of the Fityk program (version 1.3.1) were used for the deconvolution of the Raman spectra.

2.2. Characterization of the adsorbent

Several techniques were used to characterize the CAC 8X30 and thus provide information for the mathematical models (see Table 1). The data obtained embraced physical properties such as the size of pores, density, porosity, heat capacity, and chemical properties like functional groups and elemental composition.

2.3. Adsorption isotherms - monocomponent systems

The high-pressure CO_2 and CH_4 adsorption isotherms were carried out at 298 K and 323 K up to 32 bar in an automatic manometric high-pressure device HPVA II (Micromeritics), whereas the H_2O isotherms were measured at 298K and 323K up to the saturation pressure (Belsorp max II). Before any measurement, the samples were outgassed under a secondary vacuum (7×10^{-6} mbar) and 383 K for at least 48 h. After evacuation, the pressure was increased stepwise to 32 bar (CH_4 and CO_2) or up the saturation pressure (H_2O), and then stepwise decreased. At each step, the amount of gas adsorbed by the sample was calculated as the difference between the amount of gas dosed and determined at the equilibrium pressure. The contribution of the empty cell was systematically measured and subtracted from all data to improve accuracy.

2.4. Binary equilibrium experimental data

Binary equilibrium was experimentally calculated from binary breakthrough curves of the mixture of CH_4 (60 vol%) and CO_2 (40 vol%), considering the variations of flow, temperature inside the column, molar fraction of each component, and density of the gas

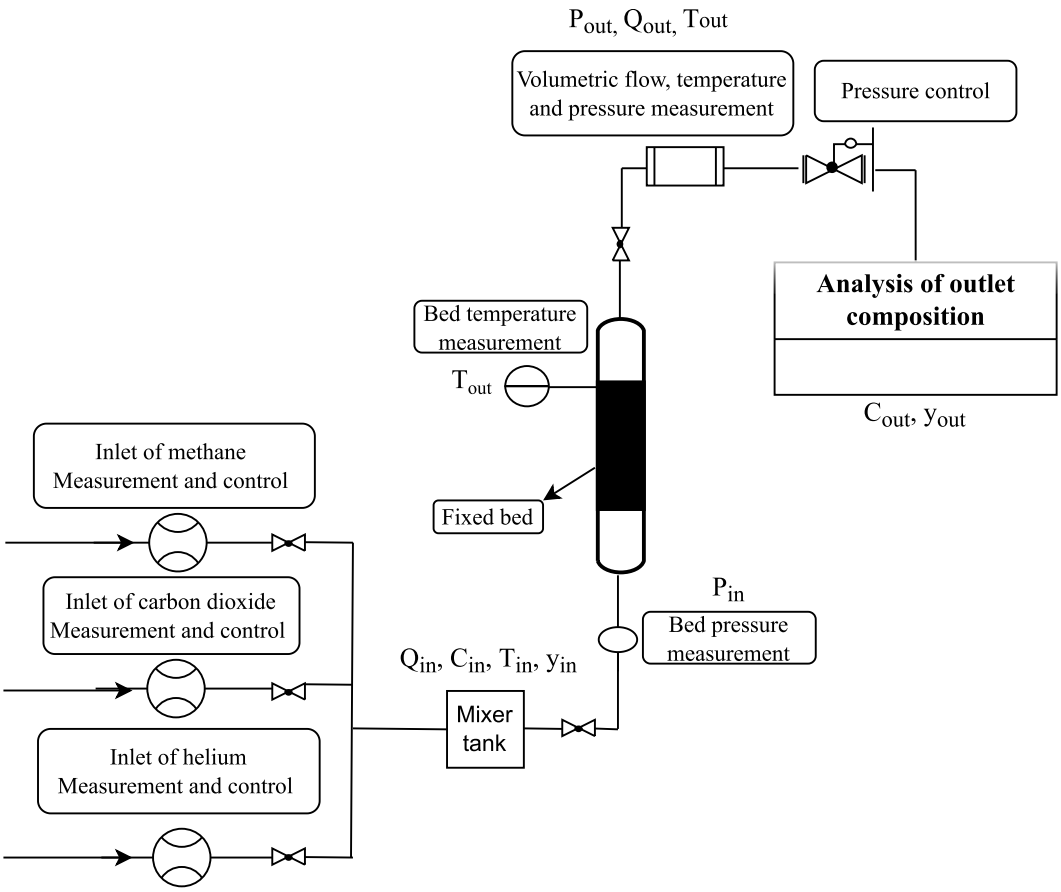

Fig. 1. Scheme of the apparatus used to obtain breakthrough curves: volumetric flow controllers and meters, solenoid valve, pressure transducer, bed temperature meter, temperature, pressure, and flow meter, backpressure regulator, and gas chromatograph.

mixture all along the curve. The adsorbed amount of each component was calculated following the mass balance presented in Eq. (1), where $C_{i,in}$ and $C_{i,out}$ were calculated by the ideal gas state equation (Eq. 2), m_{ads} was measured before packing the bed, using previously dried AC. Besides, bed porosity (ε_{bed}) was determined following Eq. (3), while particle (ρ_p) and bed density (ρ_{bed}) were calculated by Eqs. (4) and (5), respectively. True density (ρ_{true}) was obtained by Helium Pycnometry and particle porosity (ε_p) by Mercury Porosimetry.

$$q_i = \frac{\int_0^{t_{sat}} Q_{in} C_{i,in} dt - \int_0^{t_{sat}} Q_{out} C_{i,out} dt - V_{bed} C_{i,in} \varepsilon_{bed}}{m_{ads}} \tag{1}$$

$$C_i(z,t) = \frac{y_i P_i(z,t)}{RT(z,t)} \tag{2}$$

$$\varepsilon_{bed} = 1 - \left(\frac{\rho_{bed}}{\rho_p}\right) \tag{3}$$

$$\rho_p = \rho_{true}\left(1 - \varepsilon_p\right) \tag{4}$$

$$\rho_{bed} = \left(\frac{m_{bed}}{V_{bed}}\right) \tag{5}$$

Note: The physical meaning and the units for each component of Eq. (1) to Eq. (5) are described in the nomenclature table.

Besides, other parameters needed to calculate the adsorbed amount (Eq. (1)) were measured during the process at the inlet and at the outlet of the adsorption bed, namely temperature (T_{in} and T_{out}), pressure (P_{in} and P_{out}), volumetric flow (Q_{in} and Q_{out}), and molar fraction (y_{in} and y_{out}), as can be seen in the scheme of the experimental apparatus used for the breakthrough curves presented in Fig. 1.

3. Mathematical modeling

The mathematical modeling within the present work was performed by determining the equilibrium parameters from the monocomponent isotherms and then using them to predict the binary behavior. The software Gproms™ was used to estimate the equilibrium parameters and for the simulations [24].

3.1. Monocomponent equilibrium

The monocomponent equilibrium isotherms for CH_4, CO_2, and H_2O were described by the well-known models of Langmuir (L) and Multisite Langmuir (ML), whose equations are presented in Table 2.

The adsorption equilibrium constant (K_i) depends on temperature according to the Van't Hoff's equation (Eq. (6)), while the heat of adsorption can be related to the exponential term (Eq. (7)):

$$K_i = K_{1,i} e^{K_{2,i}\left(\frac{1}{T} - \frac{1}{T_{ref}}\right)} \tag{6}$$

$$\Delta H_{ads,i} = K_{2,i} R \tag{7}$$

3.2. Binary (CH_4/CO_2) and ternary ($CH_4/CO_2/H_2O$) equilibrium

The binary equilibrium prediction was carried out using the extended models of Langmuir and Multisite Langmuir (L-L and ML-ML, respectively), simulating the binary profiles through the parameters determined from the monocomponent isotherms. The compositions tested simulated the concentrations of CH_4 and CO_2 in raw biogas, which vary from 50 to 70 CH_4% and 30–50 CO_2% [2]. Besides, the Ideal Adsorbed Solution Theory (IAST) was also employed to simulate the binary isotherms, using parameters estimated from the Langmuir model (IAST-L) and the Multisite Langmuir model (IAST-ML).

For that, a reduced spreading pressure is calculated for all constituents at equilibrium by integrating the Gibbs' adsorption and using the monocomponent adsorption models shown in Table 2 since, according to IAST, the spreading pressures for all constituents at

Table 2
Isotherm models used to describe the adsorption of CH_4, CO_2, and H_2O on activated carbon.

Model	Equation	Reference
Langmuir	$\frac{q_{eq,i}}{q_{max,i}} = \frac{K_i P_i}{1 + \sum_{j=1} K_j P_j}$	[25]
Multisite Langmuir	$\frac{q_{eq,i}}{q_{max,i}} = K_i P_i \left(1 - \sum_{j=1} \frac{q_{eq,j}}{q_{max,j}}\right)^{\alpha_i}$	[26]

equilibrium are equal to the mixture spreading pressure. So, the reduced spreading pressure of a pure component in the standard state (π_i^*) is given by Eq. (8), where $q_{eq,i}$ is given by the monocomponent isotherm, while the resulting spreading pressure for two components (i and j) can be described as shown in Eq. (9) [16,27].

$$\pi_i^* = \frac{\pi_i A}{RT} = \int_0^{P_i^0} \frac{q_{eq,i}}{P_i} dP_i \tag{8}$$

$$\pi_T^* = \frac{\pi_i A}{RT} = \int_0^{P_i^0} \frac{q_{eq,i}}{P_i} dP_i = \int_0^{P_j^0} \frac{q_{eq,j}}{P_j} dP_j \tag{9}$$

The predicted values obtained using parameters estimated from monocomponent isotherms models (see Table 2) were compared with those experimentally obtained from the breakthrough curves, aiming to analyze the predictability of simulated binary curves and the reliability of the experimental data. Besides, ternary equilibrium was simulated by IAST-L by using the parameters estimated from the monocomponent isotherms of each component of the ternary mixture ($CH_4/CO_2/H_2O$). Different concentrations of water vapor, defined according to the average composition of water in raw biogas, which varies from 1 to 5 % [2], were simulated to test the effect of moisture on biogas upgrading.

Binary and ternary isotherms were also simulated for a reference adsorbent (zeolite 13X) using experimental data for adsorption equilibrium of CH_4 and CO_2 [28] and H_2O [29] on zeolite 13X from the literature to compare its behavior with that of the CAC 8X30.

3.3. Selectivity

As an indicative of the potential of the CAC 8X30 of separating the binary (absence of water vapor) and ternary mixtures (presence of water vapor), its selectivity to CO_2 over CH_4 was calculated based on the uptake of each component (q_i) and the partial pressure (p_i), as can be observed in Eq. (10). The same procedure was taken for the reference adsorbent (zeolite 13X).

$$S_{CO_2/CH_4} = \left(\frac{q_{CO_2}}{q_{CH_4}}\right)\left(\frac{p_{CH_4}}{p_{CO_2}}\right) \tag{10}$$

4. Results and discussions

4.1. Characterization

Essential information on the physical properties of the CAC 8X30 was obtained to enable the calculations of experimental binary isotherms and for the mathematical modeling of the continuous process in PSA unity in forthcoming studies. The density of the CAC 8X30 obtained by Helium Pycnometry was 1700 kg m^{-3}, while the porosity obtained by Mercury Porosimetry was 0.374.

From the Physisorption, it was possible to assess in detail the textural characteristics of the material. The Physisorption isotherms and the Pore Size Distribution (PSD) are presented in Fig. 2a and b, respectively. One may notice that there is a trimodal distribution within the micropore region (pore with ≤2 nm). In fact, the volume of micropores correspond to 94 % of the total pore volume (V_{micro}/V_T), whereas the remaining 6 % are ascribed to mesopores (V_{mes}/V_T), as can be extracted from the values of pore volume presented Table 3. Within the micropore region, 59 % are composed of ultramicropores (pore with <0.7 nm) and 41 % of supermicropores (0.7 ≤ pore with ≤ 2 nm) [30]. Besides that, the calculated overall average pore size was 1.1 nm, while the average micropore size was 0.7 nm.

These pore characteristics might contribute to the kinetic separation of gases because materials with narrow pores may successfully separate mixtures of gases when there is a difference in the kinetic diameter of the gases to be selectively adsorbed [30], as the case of

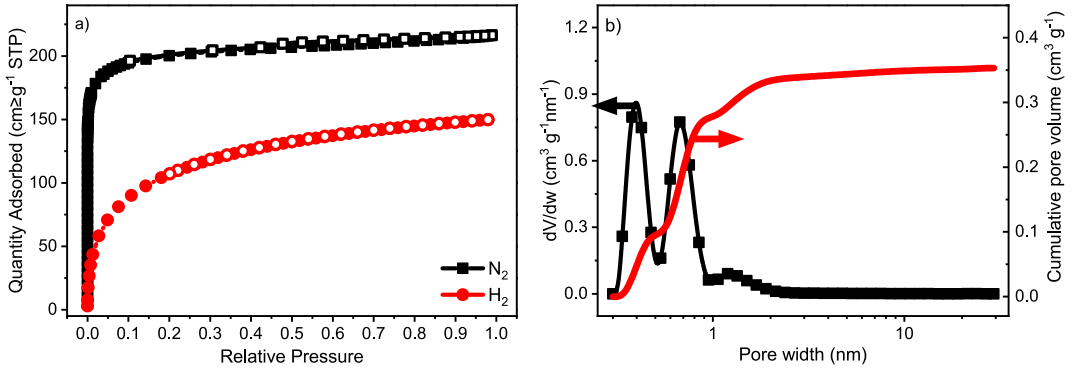

Fig. 2. Textural characterization of coconut shell activated carbon; a) N_2 and H_2 Physisorption isotherms; b) pore size distribution and cumulative pore volume.

the mixture CH_4/CO_2. Besides that, due to the high surface area found for this CAC 8X30 ($S_{NLDFT} = 1105\ m^2\ g^{-1}$), the material could also be used for other purposes, such as gas storage, as reported elsewhere [19]. On the other hand, chemical aspects also play an important role because they affect the affinity between adsorbent and adsorbate [31] and thus should be addressed.

The specific heat capacity of the CAC 8X30 was determined from the DSC, comparing the signals of a standard and the carbon material. In Fig. 3a, the DSC signals of the standard (sapphire) as well as the sample (AC) are plotted along with the signal of the empty crucible, which was used to blank correct the signals [22,23]. The temperature is also plotted to have a better understanding of the methodology. In Fig. 3b, the calculated heat capacities at different temperatures are plotted, highlighting the one at 25 °C (298 K), where a value of 1.86 $J\ K^{-1}\ g^{-1}$ was found.

The chemical properties of the CAC 8X30 were assessed in this paper by Elemental Analysis and FTIR. It can be noticed from the results presented in Table 4 that the material has high carbon content, with oxygen and nitrogen in low compositions. The carbon content is much higher than that found in other studies reported in the literature for activated carbons. According to Rattanaphan and coworkers [32], carbon atoms play an essential role in the organization of the structure of activated carbon. In contrast, nitrogen and oxygen affect the reaction that may occur on the material's surface.

The IR spectra shown in Fig. 4 were obtained for pristine activated carbon (PAC) and used activated carbon (UAC), in which UAC was submitted to several adsorption cycles (saturation and regeneration) using CH_4/CO_2 binary mixtures. Since most literature reports treat the separation of CH_4/CO_2 binary mixtures by adsorption exclusively as physical adsorption, the objective of the FTIR analysis for PAC and UAC was to investigate if there were changes in the functional groups after the contact with these adsorbates, which could indicate if there is some chemical interaction between adsorbent and adsorbates.

Activated carbons may present both acid and basic chemical characteristics. The surface acidity is related to the functional groups that contain oxygen, such as carboxyl groups, lactones, and phenols, whereas the basicity is commonly ascribed to the presence of functional groups ether, hydroxyl, and carbonyl [33]. In general, it can be said that the CAC 8X30 presents a neutral surface containing both acidic and basic groups, which is in accordance with the point of zero charge ($pH_{pzc} = 7.03$) reported elsewhere [18] for the same material.

The strong absorption band 3435 cm^{-1} can be assigned to the O–H bond stretching vibration. The 2434 cm^{-1} band was attributed to alkyne [34], while the absorption bands at 2922 cm^{-1}, 2862 cm^{-1}, and 1434 cm^{-1} refer to C–H asymmetric and symmetric stretching [35]. The band at 1728 cm^{-1} can be ascribed to C═O in ester [36], whereas the bands at 1634 cm^{-1}, 1385 cm^{-1}, 1284 cm^{-1}, 1105 cm^{-1}, and 1048 cm^{-1} are associated with asymmetric and symmetric stretching vibrations of C–O bond, present in carboxylic groups, aromatic ethers, esters, and phenols [35] of lignin. The band at 1568 cm^{-1} can be associated with C═C from alkenes [36], and one minor band at 775 cm^{-1} is related to out-of-plane deformation of C–H from aromatic structures [35]. All identified bands are summarized in Table 5.

By carefully comparing the spectra of PAC with the one of UAC, it can be noticed that there is a pronounced modification in the latter material. The band at 1568 cm^{-1} found in PAC, which refers to the C═C bond of alkenes, is no longer present in UAC after contact with methane and carbon dioxide. Besides that, there is a pronounced increase in the band's intensity at 3435 cm^{-1}, which refers to the OH group of hydroxyls [34]. The disappearance of this band might be related to some level of chemical interaction between carbon dioxide and the material's surface. So, the alkene group may have undergone oxidation by CO_2, breaking the double bond and forming new hydroxyl groups (higher intensity at 3435 cm^{-1}). On the other hand, the lower affinity of CH_4 with PAC, observed in the equilibrium isotherms (see Fig. 6), is justified by the weak interactions between methane molecules and the carbon surface (van der Waals). Thus, they are only intermolecular interactions, which are less intense than those between CAC 8X30 and CO_2.

By analyzing the Raman spectra of PAC and UAC presented in Fig. 5, one may see two well-defined peaks, near 1345 cm^{-1} and around 1595 cm^{-1}. Liu and coworkers [37] identified these same peaks for an AC used for adsorption of sulfamethazine. The authors indicated that the peak near 1345 cm^{-1} may be caused by reasons such as low symmetry, arrangement of the carbon structure, and lattice defects. On the other hand, the peak near 1595 cm^{-1} may be ascribed to graphite. Comparing the spectra of PAC and UAC (Fig. 5), one cannot define any relevant difference by the Raman technique.

4.2. Monocomponent equilibrium

As expected, the equilibrium experimental data showed that the amount of CO_2 adsorbed was much higher than that of CH_4 within the assessed pressure range, which means that the adsorption capacity of the CAC 8X30 for the carbon dioxide is much higher (see Fig. 6). By taking points for the adsorbed amount of CO_2 and CH_4 from the monocomponent adsorption isotherms at 298 K at different pressures, one may achieve ratios (qCO_2/qCH_4) of 2.5, 1.7, and 1.6, at the beginning (1 bar), in the middle (15 bar), and at the end (30 bar) of the tested pressure range. This behavior has already been reported in other studies on activated carbons [1,15,38] and might indicate the material's potential to separate the gaseous mixture even at low pressure.

Table 3
Textural properties of the coconut shell activated carbon. Surface area (S_{NLDFT}), total pore volume (V_T), mesopore volume (V_{mes}), micropore volume (V_{micro}), ultramicropore volume ($V_{ult\text{-}micro}$), supermicropore volume ($V_{sup\text{-}micro}$), average pore size (L_0) and average micropore size ($L_{0\text{-}micro}$).

Textural Properties							
S_{NLDFT} [$m^2\ g^{-1}$]	V_T [$cm^3\ g^{-1}$]	V_{mes} [$cm^3\ g^{-1}$]	V_{micro} [$cm^3\ g^{-1}$]	$V_{ult\text{-}micro}$ [$cm^3\ g^{-1}$]	$V_{sup\text{-}micro}$ [$cm^3\ g^{-1}$]	L_0 [nm]	$L_{0\text{-}micro}$ [nm]
1105	0.35	0.02	0.34	0.20	0.14	1.1	0.7

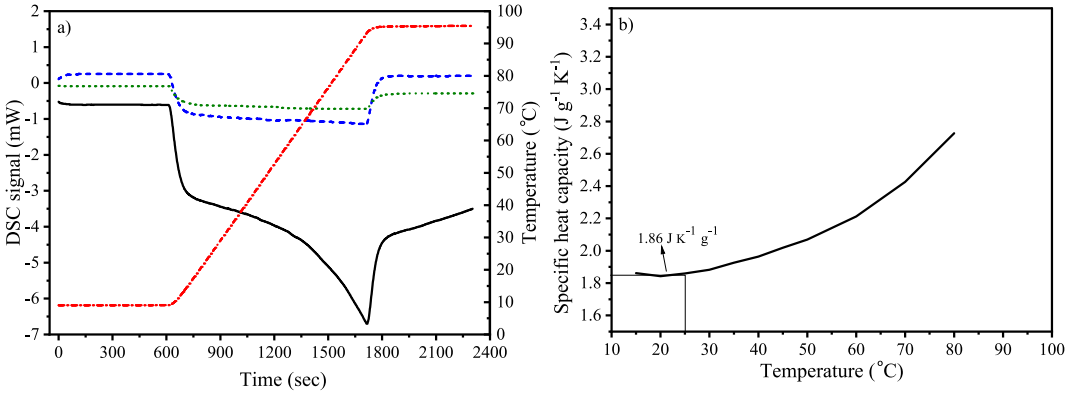

Fig. 3. Specific heat capacities calculated from DSC signals; a) DSC signals; — Coconut shell activated carbon; --- Sapphire (standard); ····· Blank (empty crucible); —·— Temperature; b) Specific heat capacities of coconut shell activated carbon in relation to temperature.

Table 4
Elemental Analysis of the coconut shell activated carbon.

Elemental Analysis				
C [wt. %]	H [wt. %]	S [wt. %]	O [wt. %]	N [wt. %]
93.8	0.84	0.0	4.9	0.46

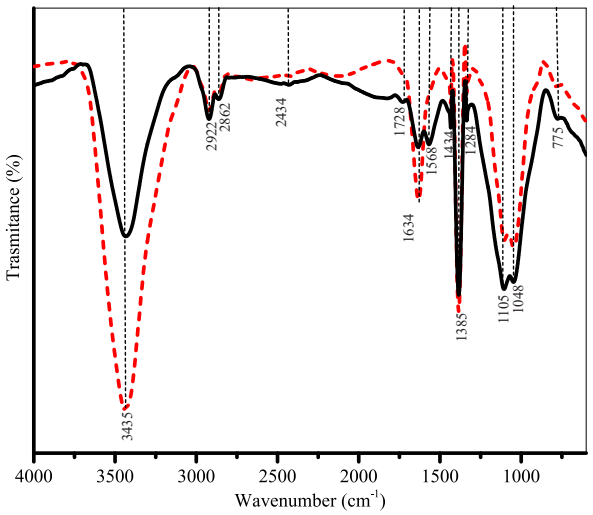

Fig. 4. FTIR spectra of coconut shell activated carbon. – Pristine activated carbon (PAC); ---Used activated carbon (UAC).

In Table 6, a comparison with the adsorption capacities at low pressure (P = 1 bar) found in other studies can be observed. Besides, the values for q_{max}, $\Delta H_{ads,i}$, and Ki (which is a function of K_1 and K_2 - see Eq. (6) and Eq. (7)), were all higher for carbon dioxide when compared to methane (see Table 7). Although there were indications of chemical interaction between CO_2 and CAC 8X30 in the FTIR analysis, there is no pronounced difference between the values of heat of adsorption for CH_4 and CO_2, so the uptake of both adsorbates is mainly due to Physisorption rather than Chemisorption. As could be concluded from the FTIR results reported here and from pH_{pzc} reported elsewhere [18], the CAC 8X30 presents basic groups that may facilitate the CO_2 adsorption. Overall, less acidic AC tend to have their CO_2 adsorption capacity favored [39], which may explain the higher affinity observed between CAC-CO_2 than between CAC-CH_4.

Regarding the mathematical models used to describe the monocomponent isotherms, one may notice by observing Fig. 6 that both Langmuir and ML models showed good agreement with the experimental data up to approximately 8 bar, whereas at higher pressures (P > 8), ML described the experimental data better. It is worth mentioning that the ML isotherm considers that one single molecule can occupy more than one adsorption site, differently from the Langmuir isotherm (one molecule occupies only one site). This assumption is taken into account by using the parameter α, which is defined as the number of sites or equivalent spaces occupied by the component.

Table 5
Summary of FTIR spectra found for pristine and used activated carbons.

Wavenumber	Assignments	Functional groups
3435	O–H stretching	Hydroxyl
2922	C–H asymmetric and symmetric stretching and axial deformations	Alkane
2862		
1434		
2434	C ≡C stretching bond	Alkyne
1728	C═O stretching	Ester
1634	C–O symmetric and asymmetric axial deformation vibrations	Carboxylic acids, aromatic ethers, esters and phenols
1385		
1284		
1105		
1048		
1568	C═C stretching band	Alkene
775	C–H out-of-plane deformation	Aromatic ring

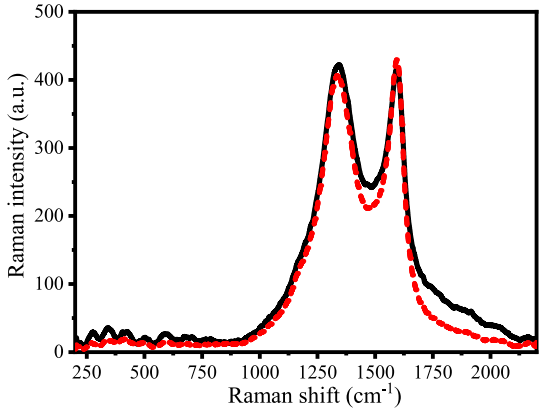

Fig. 5. Raman spectra of pristine and used coconut shell activated carbon. – Pristine activated carbon (PAC); --- Used activated carbon (UAC).

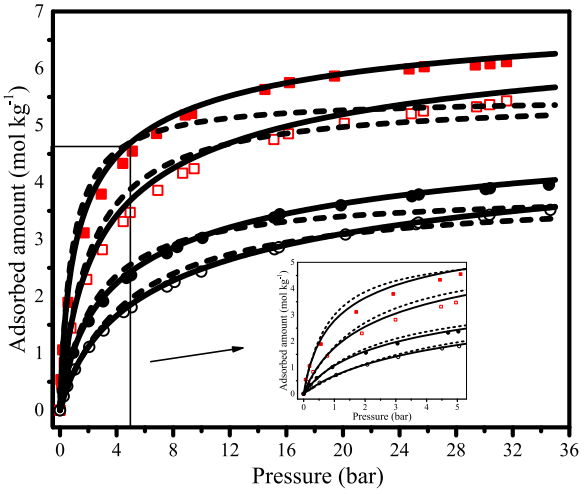

Fig. 6. Monocomponent adsorption isotherms of CO_2 and CH_4 on coconut shell activated carbon. ■ CO_2 at 298 K; □ CO_2 at 323 K; ● CH_4 at 298 K; ○ CH_4 at 323 K; — Multisite Langmuir model; — Langmuir model.

So, a larger molecule should have a larger alpha on the same surface, which is in line with the alpha values shown in Table 7.

Although the ML isotherm also considers adsorption on a homogeneous surface and that there are no interactions between the adsorbate molecules, it has been effectively employed to describe systems in which the adsorbent surface sites are heterogeneous such as activated carbons, zeolites, and carbon molecular sieves [26,30,40]. This can be attributed to the fact that the heterogeneity of the adsorbent surface sites may affect the value for α, and thus allow a good description, even if empirical, of the adsorption equilibrium

Table 6
Literature values for the adsorbed amount of carbon dioxide and methane by activated carbons at equilibrium, at 1 bar and 293 K.

q_{CO2} (mol kg^{-1})	q_{CH4} (mol kg^{-1})	Reference
2.21	0.87	Present paper
2.10	0.54	[1]
2.20	1.14	[16]
2.76	1.25	[15]

Table 7
Equilibrium parameters estimated from monocomponent isotherms of CH_4 and CO_2 on CAC 8X30 at temperatures from 298 to 323 K and pressures from 0 to 35 bar.

Model	Adsorbate	q_{max} (mol kg^{-1})	K_1 (bar^{-1})	K_2 (K)	α^a	ΔH_{ads} (kJ mol^{-1})
Langmuir	CO_2	5.48	3.54	3504.63	–	29.14
Multisite Langmuir		7.59	2.76	3394.67	2.14	28.22
Langmuir	CH_4	3.82	0.88	2524.48	–	20.99
Multisite Langmuir		6.24	0.60	2465.85	2.61	20.50

[a] To assure thermodynamic consistency, the product α. q_{max} was maintained for both adsorbates (α. $q_{max}(CO2) = \alpha$. $q_{max}(CH4)$) in the model of Multisite Langmuir.

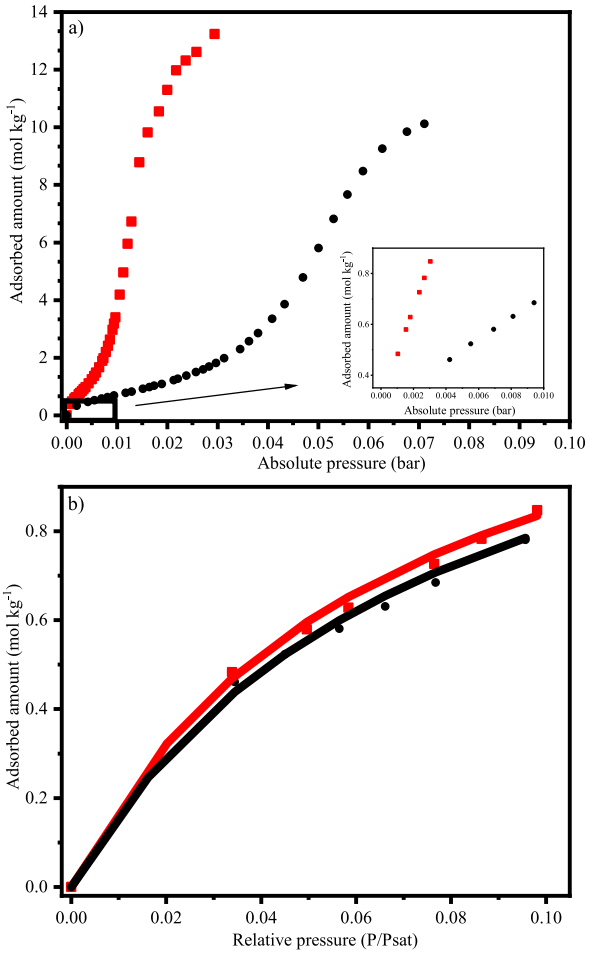

Fig. 7. Monocomponent adsorption isotherms of H_2O on coconut shell activated carbon. a) up to the saturation pressure; b) up to 10 % of the saturation pressure (P/Psat = 0.1); ■ 298 K; ● 323 K; — Langmuir model.

[40]. In general, it can be concluded that the estimated parameters from both Langmuir and ML may be employed to design a continuous adsorption process such as PSA at low pressures, whereas, at pressures higher than 8 bar, the latter model would be preferable.

By analyzing the water vapor isotherm presented in Fig. 7a, one may see a high uptake of H_2O by the CAC 8X30 at very low pressures. In fact, the saturation pressures (Psat) for the adsorption isotherms at 298 K and 323 were 3.1×10^{-2} and 1.2×10^{-1} bar, respectively. Besides that, as expected for an exothermic process, the uptake was clearly higher at the lowest temperature within the complete pressure range, as can be seen in the zoomed part of the graph, which corresponds to the isotherm region from 0 to 10 % of the saturation pressure (P/Psat = 0.1).

Considering that the water vapor concentration in raw biogas varies from 1 to 5 vol %, the adsorption equilibrium parameters of H_2O on CAC 8X30 were estimated using the limited region of the isotherm (up to P/Psat = 0.1). As can be observed in Fig. 7b, where the experimental and simulated data are plotted against relative pressure up to 0.1, the Langmuir model showed a good fit to the experimental data, generating the following estimated parameters: $q_{max} = 1.42$ mol kg^{-1}, $K_1 = 2.77 \times 10^3$ bar^{-1}, and $K_2 = 5.77 \times 10^3$ K. Moreover, the heat of adsorption for H_2O on CAC 8X30 was 47.9 kJ mol^{-1}, which is slightly higher than the value of 43.9 kJ mol^{-1} found elsewhere for the system pine sawdust-based activated carbon and water vapor [17].

4.3. Binary equilibrium (CH_4/CO_2) and selectivity

Experimental binary isotherms were obtained from kinetic binary breakthrough curves from 1 to 5 bar at 298 K and compared with simulated binary isotherms. By observing the values of adsorption capacities (i.e., equilibrium points of the kinetic curves) shown in Table 8, one may notice that there is a preference to adsorb CO_2 over CH_4 in a mixture of CH_4 (60 vol%) and CO_2 (40 vol%), as expected. In fact, as can be seen in the zoomed part of Fig. 6, the adsorption of carbon dioxide is considerably higher than that of methane, even at low pressures.

In Fig. 8a, the experimental values are plotted along with the simulations of the binary mixture made from parameters obtained from pure gas isotherms, which were performed using IAST in conjunction with the Langmuir model (IAST-L) and ML (IAST-ML) and by using the single models (Langmuir and ML). One may notice that the IAST fits become less accurate as pressure increases. This was also observed by Vilella and coworkers [16] and may be explained by the fact that at higher pressures, the interactions in the adsorbed phase may become dominant at high surface coverage applicability, thus reducing the reliability of IAST.

Moreover, the simulations are, in general, more accurate in describing the CO_2 behavior, presenting average standard deviations for CO_2 adsorption from 3 to 5 % for IAST-L, Langmuir, IAST-ML, and ML (the last two models provided practically identical results so that they overlaid each other in the graphic). Durán and coworkers [17] observed that the uptake of CH_4 from a binary mixture by a saw-dust-based activated carbon is probably more affected than that of CO_2. The experimental and simulated total amount adsorbed ($CH_4 + CO_2$) can also be observed in Fig. 8b, confirming the good agreement between experimental and simulated curves.

Considering the low deviation between the simulations using parameters from monocomponent isotherms (mainly IAST-L) and the experimental uptake calculated from binary breakthrough curves, these estimated equilibrium parameters are strongly reliable, and the model can be used to predict the binary equilibrium of adsorption for different compositions, temperatures, and pressures, which allows in turn, the calculation of the selectivity.

In Fig. 9a, binary isotherms simulated from 0 to 5 bar at 298 K for three different CH_4/CO_2 vol% compositions can be observed. It can be noted that, as expected, the higher the composition, the higher the absolute uptake by the AC. So, the greatest CH_4 uptake occurs for the 70-30 vol% composition, while the greatest uptake of CO_2 happens for the composition of 50-50 vol%. At all compositions, however, the adsorption capacity of CO_2 exceeded that of CH_4.

The selectivity of the CAC 8X30 for CO_2 with pressure increase was calculated by IAST-L and is presented in Fig. 9b, wherein it can be observed that selectivity increases with total pressure up to 5 bar for all tested compositions. This makes sense since although the slope strongly declines after 3 bar on the monocomponent isotherms for both adsorbates (see Fig. 6), there is no well-defined plateau at 5 bar yet. Villela and coworkers [16] also achieved this profile for the selectivity of CO_2 over CH_4 s (70-30 vol%, CH_4/CO_2) at 293 K using a coconut-based activated carbon. However, the selectivity calculated based on IAST-Toth prediction in the cited study at 1 bar was slightly lower than 2, while in the present study, it was 4.7 (calculated based on IAST-L predictions).

The CAC 8X30 presents thus a high equilibrium selectivity for CO_2 over CH_4, which may indicate a good potential to be applied in separation processes such as PSA. However, it must be kept in mind that these results were achieved using synthetic mixtures, neglecting the presence of minor contaminants such as water vapor and considering only the major compounds of raw biogas.

Table 8
Experimental equilibrium results obtained from CH_4/CO_2 (60-40 vol%) breakthrough curves at T = 298 K and Q = 0.5 L min^{-1} (T = 298 K and P = 1 bar).

Total pressure (bar)	Partial pressure (bar)		q_{eq} (mol kg^{-1})		q_{tot} (mol kg^{-1})
	CH_4	CO_2	CH_4	CO_2	
1	0.6	0.4	0.4	1.5	1.9
2	1.2	0.8	0.6	2.1	2.7
3	1.8	1.2	0.8	2.7	3.5
4	2.4	1.6	1.0	3.1	4.1
5	3.0	2.0	1.2	3.3	4.5

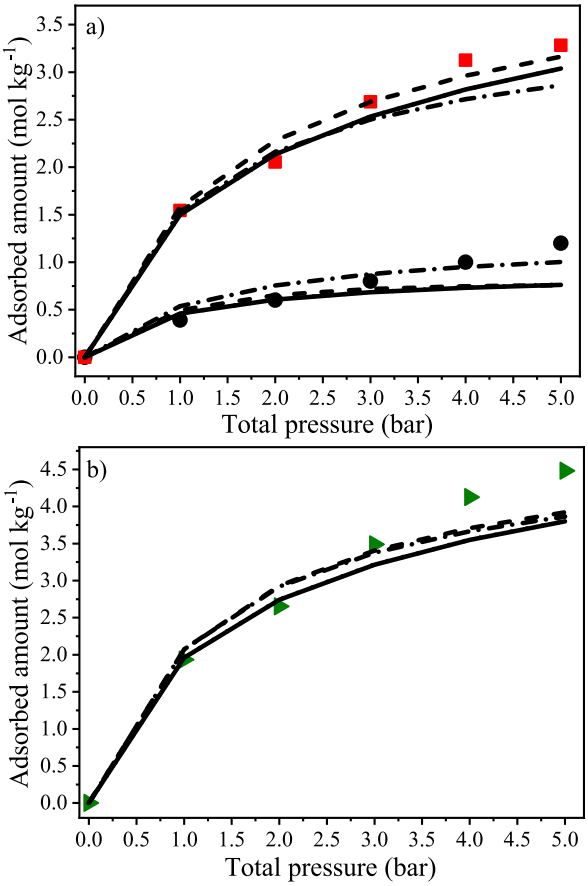

Fig. 8. Predicted and experimental binary adsorption isotherms for a mixture of CH_4 (60 vol%) and CO_2 (40 vol%) at 298 K on coconut shell activated carbon; ■ CO_2, ● CH_4; (a) adsorbed amount of each component separately; (b) total adsorbed amount; ▶ $CO_2 + CH_4$, — IAST-ML, —— IAST-L, ... •Multisite Langmuir, —•— Langmuir.

Therefore, simulations including water vapor were conducted to assess the material's behavior in wet conditions.

4.4. *Ternary equilibrium ($CH_4/CO_2/H_2O$) and selectivity*

The IAST-L model was further employed to simulate ternary equilibrium uptake, including the presence of water vapor, and using the parameters estimated from the monocomponent H_2O isotherms (see section 3.1). As can be seen in Fig. 10, the adsorbed amount of H_2O is high even at low pressures due to its very high affinity with the AC (see values of *K1* und *K2* in section 4.2) and decreases with increasing pressure, while the amount of adsorbed CH_4 and CO_2 increases with pressure like in the dry (binary) system. By applying K_1 and K_2 estimated from the Langmuir isotherm in Equation (6) and taking as example the temperature of 298 K, one achieves the equilibrium constants for CO_2 (K = 1.21 bar^{-1}), CH_4 (K = 0.41 bar^{-1}) and H_2O (475.9 bar^{-1}), which clearly shows that the affinity of water vapor to CAC 8X30 is significantly higher.

CO_2 adsorption on ACs at low to moderate pressures is often negatively affected by the presence of H_2O, due to the strong affinity of water with surface functional groups of ACs [41]. By quantitatively comparing the binary isotherms (dry conditions, Fig. 9) with the ternary isotherms (wet conditions, Fig. 10), it can be seen that the adsorbed amount of both methane and carbon dioxide reduced in the presence of water vapor (3 wt% in Fig. 10), as expected. Taking specifically the simulated uptake for a wet ternary mixture of ($CH_4/CO_2/H_2O$, 58.2/38.8/3.0 vol%) in comparison with the dry binary mixture (CH_4/CO_2, 60-40 vol%), the decrease was 64 % for CH_4 and 60 % for CO_2 at 1 bar. At 5 bar, the reductions corresponded to 41 % and 38 %, respectively.

According to the model proposed by Do and Do [42], water vapor molecules get adsorbed onto functional groups by chemisorption and chemisorbed water might then form a site for further water adsorption by hydrogen bonding forming thus clusters. When the concentration of water vapor within these cluster reaches a certain threshold, the molecules are finally adsorbed into the micropores. However, at high pressures, the presence of pre-adsorbed water can promote the uptake of CO_2 even through mechanisms other than adsorption, including dissolution and hydrate formation [41]. In the present study, however, the pressure range is low to moderate, which explains the negative influence on CH_4 and CO_2 adsorption in the presence of water vapor.

On the other hand, since the adsorption of CH_4 seems to be more affected by the presence of water vapor, the selectivity of the AC

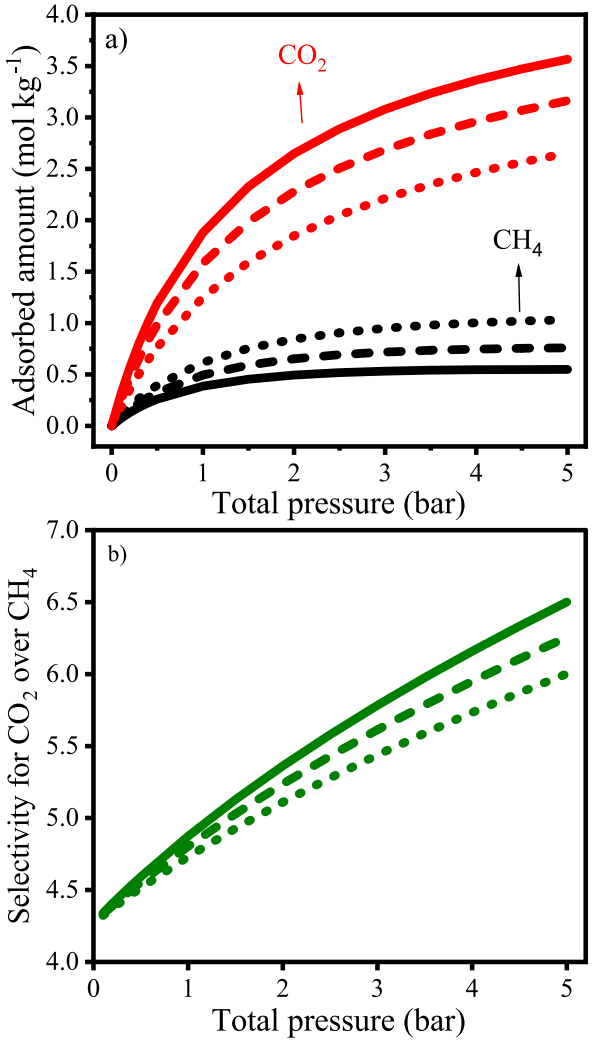

Fig. 9. Simulated binary isotherms (a) and selectivities for CO_2 over CH_4 (b) for different compositions of the binary mixture CH_4/CO_2 on coconut shell activated carbon at 298 K (CH_4/CO_2: 50-50 vol%; —— 60-40 vol%; and ... •70-30 vol%.

8X30 for CO_2 over CH_4 tends to become even higher with increasing water vapor concentration (from 1 to 5 wt%) within the simulated pressure range for all simulated biogas compositions. This can be seen in Fig. 11, where the selectivity for mixtures containing water vapor is compared with that of dry CH_4/CO_2 mixtures of 50/50 vol% (Figs. 11a), 60/40 vol% (Fig. 11b), and 70/30 vol% (Fig. 11c). Thus, the presence of water vapor caused a reduction in the adsorption capacity of the AC 8X30 for both major compounds of biogas, but the selectivity towards CO_2 was facilitated in comparison with the dry case.

Durán and coworkers [17] also reported such behavior for the adsorption of CH_4 and CO_2 by a pine sawdust-based activated carbon in the presence of moisture. In their study, the authors concluded that even reducing the adsorption capacity for CO_2 in the presence of moisture, the activated carbon showed great potential and could thus provide the upgrading of biogas without the need for a complete water removal prior to the adsorption unit. In fact, reference materials such as zeolite 13X may present a much greater selectivity towards CO_2 in dry conditions, but the presence of small concentrations of water may impair the removal of CO_2 from biogas because of the high affinity and high adsorption capacity of zeolite 13X for H_2O even at low partial pressures [29].

To demonstrate this behavior and compare it with that of the CAC 8X30, adsorption equilibrium experimental on zeolite 13X were taken from the literature data for CH_4, CO_2, and H_2O (see Table 9). For the estimation of the equilibrium parameters, the same procedure described in sections 3.1 and 4.2 was followed. By analyzing the estimated parameters presented in Table 9, one may notice that both adsorption capacity ($q_{max,i}$) and affinity ($K_i = f(K_{1,i}, K_{2,i}, T_i)$) are much higher for H_2O than for the other adsorbates. Although it was also observed for the CAC 8X30, the values estimated for zeolite 13X are at least one order of magnitude greater than those estimated for the activated carbon. Using the estimated parameters *K1* and *K2* to calculate the affinity of the materials with water at 298 K (see Eq. (6)), we achieved 7.9×10^3 and 4.7×10^2 for zeolite and activated carbon, respectively. On the other hand, the affinities for CH_4 and CO_2 were in the order of 10^{-2} (13X) and 10^{-1} (AC) for CH_4 and of order 1 for CO_2 for both materials.

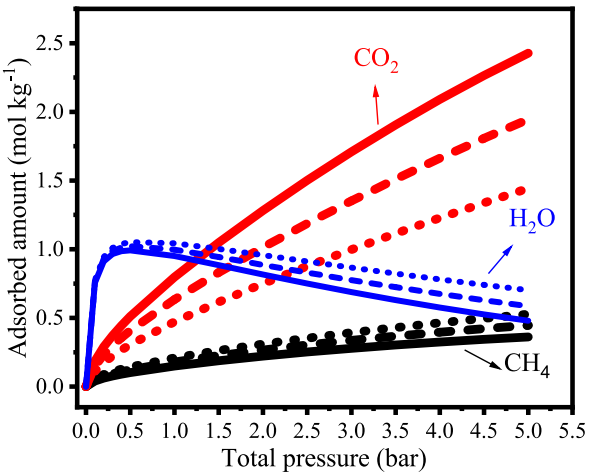

Fig. 10. Simulated ternary isotherms of adsorption of the ternary mixture ($CH_4/CO_2/H_2O$) on CAC 8X30 at 298 K. $CH_4/CO_2/H_2O$: 48.5/48.5/3.0 vol%; —— 58.2/38.8/3.0 vol%; and ... •67.9/29.1/3.0 vol%.

As shown in Fig. 12a, the reference material presents a high adsorption capacity for CO2 and provides a high selectivity for CO2 over CH4 in dry conditions. However, the presence of 3 % water vapor caused a pronounced reduction of selectivity (Fig. 12b), unlike the behavior simulated for AC 8X30, when selectivity increases with the presence of water vapor (Fig. 11). Taking as a quantitative example the simulated selectivities for zeolite 13X at 298 K, it was noticed that the values reduce from 44 (dry) to 14.5 (3 % water vapor) and from 40 (dry) to 9.8 (3 % water vapor) at 1 and 5 bar, respectively.

It is to be noticed that although the simulated selectivity of zeolite 13X in wet condition seems to be even higher than that of AC 8X30 (e.g., 11.1 and 6.1 for zeolite 13X and CAC 8X30, respectively, at 3 bar, 298 K, and 3 wt%), it does not mean that the reference material presents a good behavior in the presence of water vapor. In fact, by evaluating this result along with the adsorption capacity of CO_2, one may notice that almost no CO_2 uptake can be performed by the zeolite 13X in wet conditions within the complete tested pressure range ($CH_4/CO_2/H_2O$, 58.2/38.8/3.0 vol%). For the same system, the carbonaceous material presents a pronounced adsorption capacity for CO_2 even with the presence of water vapor (e.g., 1.9 mol kg^{-1} at 5 bar, see Fig. 10). Even when summed, the uptake of CH_4 and CO_2 by the zeolite 13X are in order of 10^{-6} mol kg^{-1}. In contrast, the adsorption capacity for H_2O is around 14.7 mol kg^{-1}, as shown in Fig. 12c. This represents a reduction in the CO_2 adsorption capacity of more than 99 % compared with the dry (binary) scenario.

Thus, zeolite 13X would not be suitable for upgrading humid biogas, while the CAC 8X30 could be employed without requiring complete water removal before the adsorption unit. On the other hand, the simulations performed for dry (binary) conditions showed higher values for selectivity and CO_2 adsorption capacity for zeolite 13X than for the CAC 8X30, as expected. Hence, further studies, including kinetic experimental data and modeling, may indicate the suitability of integrating both materials to upgrade biogas containing minor contaminants such as water vapor, either as hybrid or as separate adsorption beds.

5. Conclusions

The present paper has shown the potential of a coconut-shell activated carbon (CAC 8X30) to remove CO_2 from biogas in dry (CH_4/CO_2) and wet ($CH_4/CO_2/H_2O$) conditions. The adsorbent presents a higher adsorption capacity of CO_2 compared with CH_4 within the complete tested pressure range. Binary experimental data confirmed the good prediction capacity of the IAST-Langmuir model as well as the preference of the material for removing CO_2 from the binary mixture. Besides, the material presents high microporosity, which might favor a kinetic separation of the CH_4/CO_2 mixture in a continuous process.

By simulating ternary isotherms with the presence of moisture, it was found that, despite the reduction in CO_2 uptake, the CAC 8X30 shows excellent potential in CO_2 removal from a biogas stream, with an increase in selectivity in the presence of water vapor. On the other hand, zeolite 13X was not able to remove CO_2 from ternary mixtures but showed a higher selectivity in dry (binary) conditions. Thus, it was evidenced that CAC 8X30 could be employed for the upgrading of biogas without the need for water removal before the adsorption unit, but a higher selectivity might be achieved by integrating the use of the carbonaceous material with the zeolite 13X.

Further studies on the kinetic of CO_2 removal, including experimental data and modeling, are required to better evaluate the suitability of the tested activated carbon in continuous operation mode and the viability of integrating the use of both materials for the upgrading of biogas containing water vapor in cyclic processes such as PSA.

Funding

National Council for Scientific and Technological Development (Proc. 313734/2021-6), BRF S.A., International Center of

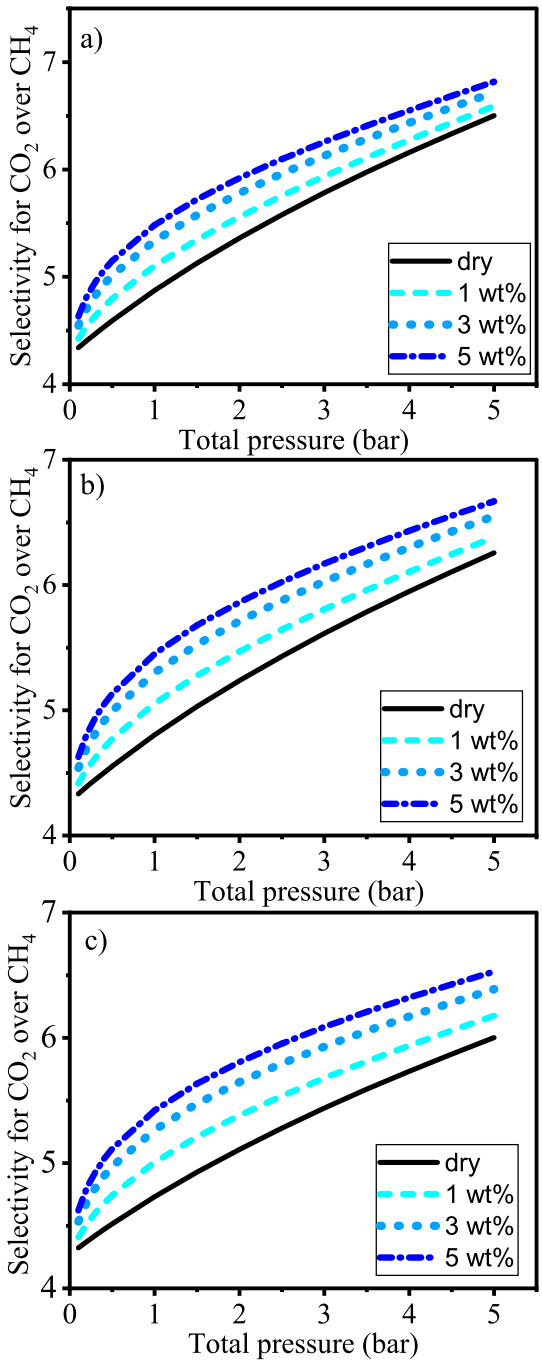

Fig. 11. Simulated selectivities of CAC 8X30 for CO_2 over CH_4 at 298 K for dry (CH_4/CO_2) and wet ($CH_4/CO_2/H_2O$) conditions: a) dry (binary) composition 50/50 vol%, b) dry (binary) composition 60/40 vol%, and c) dry (binary) composition 70/30 vol%.

Table 9
Equilibrium parameters estimated from the fit of the Langmuir model to H_2O monocomponent isotherms on zeolite 13X at temperatures from 293 K to 313K.

Adsorbate	q_{max} (mol kg^{-1})	*K1* (bar^{-1})	*K2* (K)	ΔH_{ads} (kJ mol^{-1})	Experimental data
CO_2	6.76	1.63×10^{1}	4.40×10^{3}	36.6	[28]
CH_4	6.08	1.47×10^{-1}	1.94×10^{3}	16.2	[28]
H_2O	14.81	3.57×10^{4}	5.82×10^{3}	48.4	[29]

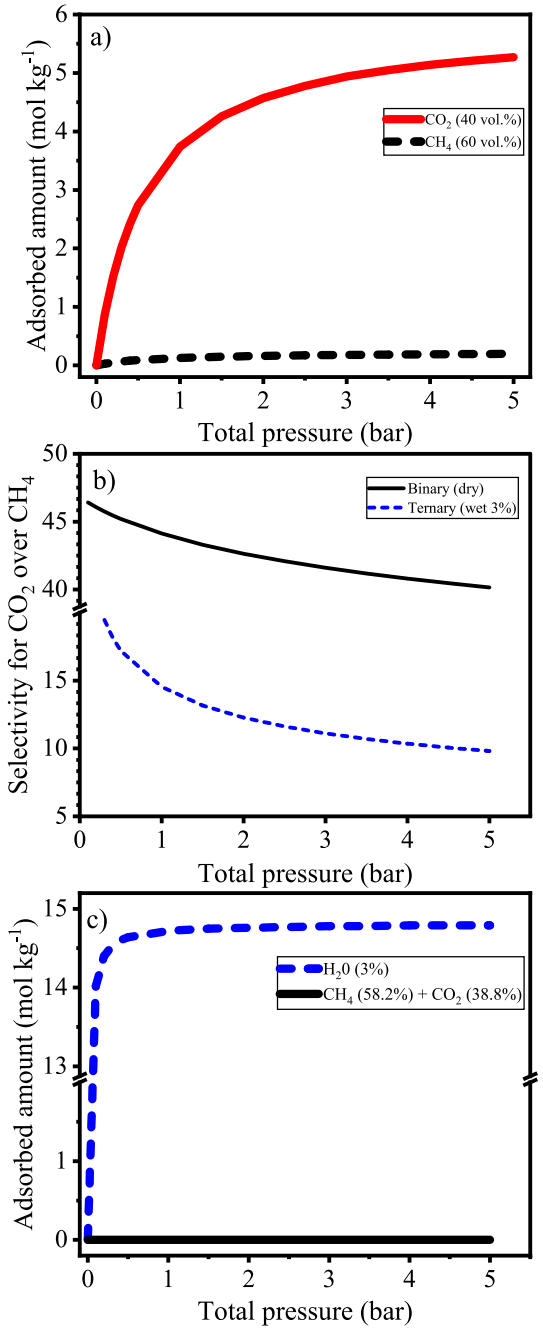

Fig. 12. Simulated adsorption profiles for zeolite 13X at 298 K: a) adsorbed amount for a binary (dry) mixture of CH_4/CO_2 (60/40 vol%); b) selectivities for CO_2 over CH_4 for dry (CH_4/CO_2) and wet ($CH_4/CO_2/H_2O$) conditions; c) adsorbed amount in a ternary (dry) mixture of $CH_4/CO_2/H_2O$ (58.2/38.8/3.0 vol%).

Renewable Energies – Biogas (CIBiogás), and Araucária Foundation (Proc. PBA202211000083).

Data availability statement

Data associated with this study has not been deposited into any publicly repository. All data relevant to this study have been

included in the paper. Additional data might be provided upon request.

Nomenclature table

Symbols	Meaning
$C_{i,in}$	Feed concentration of component i [mol L^{-1}]
$C_{i,out}$	Outlet concentration of component i [mol L^{-1}]
K_i	Equilibrium constant for component i [bar^{-1}]
$K_{1,i}$	Pre-exponential constant for the temperature dependence of K_i [bar^{-1}]
$K_{2,i}$	Exponential term for the temperature dependence of K_i [K]
m_{ads}	Mass of adsorbent [kg]
P	Pressure [bar]
$q_{eq,i}$	Adsorbed concentration in equilibrium of component i [mol kg^{-1}]
$q_{\max,i}$	Maximum adsorption capacity of component i [mol kg^{-1}]
$Q_{i.in}$	Volumetric flow of component i at the inlet of the column [L min^{-1}]
$Q_{i.out}$	Volumetric flow of component i at the outlet of the column [L min^{-1}]
R	Ideal gas constant [kJ mol^{-1} K^{-1}]
T	Temperature [K]
T_{ref}	Reference temperature [K]
V_{bed}	Volume of the bed [L]
y_i	Molar fraction of component i
y_{in}	Inlet molar fraction
y_{out}	Outlet molar fraction
Greek letters	**Meaning**
α	Number of adsorbent sites occupied by the adsorbate molecule
$\Delta H_{ads,i}$	Heat of adsorption for component i [kJ mol^{-1}]
ε_{bed}	Porosity of the fixed bed
ε_p	Porosity of the particle
ρ_{bed}	Bed density [kg m^{-3}]
ρ_p	Particle density [kg m^{-3}]
ρ_{true}	True density [kg m^{-3}]

CRediT authorship contribution statement

Junior Staudt: Writing – review & editing, Writing – original draft, Validation, Software, Methodology, Investigation, Data curation, Conceptualization. **Cassiano Moreira Musial:** Validation, Software, Investigation. **Rafael Canevesi:** Investigation, Conceptualization. **Vanessa Fierro:** Conceptualization. **Caroline Ribeiro:** Investigation. **Helton José Alves:** Conceptualization. **Carlos Eduardo Borba:** Writing – review & editing, Supervision, Software, Project administration, Methodology, Funding acquisition, Formal analysis, Conceptualization.

Declaration of competing interest

The authors declare that they have no known competing financial interests or personal relationships that could have appeared to influence the work reported in this paper.

Acknowledgments

The authors thank the Institute Jean Lamour (IJL), Épinal - France, for technical and laboratory support.

References

[1] R.B. Rios, F.M. Stragliotto, H.R. Peixoto, A.E.B. Torres, M. Bastos-Neto, D.C.S. Azevedo, C.L. Cavalcante, Studies on the adsorption behavior of CO2-CH4 mixtures using activated carbon, Braz. J. Chem. Eng. 30 (2013) 939–951, https://doi.org/10.1590/S0104-66322013000400024.
[2] R. Kapoor, P. Ghosh, M. Kumar, V.K. Vijay, Evaluation of biogas upgrading technologies and future perspectives: a review, Environ. Sci. Pollut. Control Ser. (2019), https://doi.org/10.1007/s11356-019-04767-1.
[3] L.A. Pellegrini, G. De Guido, S. Langé, Biogas to liquefied biomethane via cryogenic upgrading technologies, Renew. Energy 124 (2017) 75–83, https://doi.org/10.1016/j.renene.2017.08.007.
[4] M. Pöschl, S. Ward, P. Owende, Evaluation of energy efficiency of various biogas production and utilization pathways, Appl. Energy 87 (2010) 3305–3321, https://doi.org/10.1016/j.apenergy.2010.05.011.
[5] J. Li, J. Yang, R. Krishna, J. Li, Experiments and simulations on separating a CO2/CH4 mixture using K-KFI at low and high pressures, Microporous Mesoporous Mater. 184 (2014) 21–27, https://doi.org/10.1016/j.micromeso.2013.09.026.
[6] C. Song, Z. Fan, R. Li, Q. Liu, Y. Kitamura, Efficient biogas upgrading by a novel membrane-cryogenic hybrid process: experiment and simulation study, J. Membr. Sci. 565 (2018) 194–202, https://doi.org/10.1016/j.memsci.2018.08.027.
[7] Y. Li, L. Wang, X. Hu, P. Jin, X. Song, Surface modification to produce superhydrophobic hollow fiber membrane contactor to avoid membrane wetting for biogas purification under pressurized conditions, Sep. Purif. Technol. 194 (2018) 222–230, https://doi.org/10.1016/j.seppur.2017.11.041.
[8] C.E. Wylock, W.M. Budzianowski, Performance evaluation of biogas upgrading by pressurized water scrubbing via modelling and simulation, Chem. Eng. Sci. 170 (2017) 639–652, https://doi.org/10.1016/j.ces.2017.01.012.
[9] W.M. Budzianowski, C.E. Wylock, P.A. Marciniak, Power requirements of biogas upgrading by water scrubbing and biomethane compression: comparative analysis of various plant configurations, Energy Convers. Manag. 141 (2017) 2–19, https://doi.org/10.1016/j.enconman.2016.03.018.
[10] L.A.M. Rocha, K.A. Andreassen, C.A. Grande, Separation of CO2/CH4 using carbon molecular sieve (CMS) at low and high pressure, Chem. Eng. Sci. 164 (2017) 148–157, https://doi.org/10.1016/j.ces.2017.01.071.

[11] P. Hao, Y. Shi, S. Li, X. Zhu, N. Cai, Correlations between adsorbent characteristics and the performance of pressure swing adsorption separation process, Fuel 230 (2018) 9–17, https://doi.org/10.1016/j.fuel.2018.05.030.
[12] S. Singhal, S. Agarwal, S. Arora, P. Sharma, N. Singhal, Upgrading techniques for transformation of biogas to bio-CNG: a review, Int. J. Energy Res. 41 (2017) 1657–1669, https://doi.org/10.1002/er.3719.
[13] C.A. Grande, R. Blom, K.A. Andreassen, R.E. Stensrød, Experimental results of pressure swing adsorption (PSA) for pre- combustion CO 2 capture with metal organic frameworks, Energy Proc. 114 (2017) 2265–2270, https://doi.org/10.1016/j.egypro.2017.03.1364.
[14] Brascarbo Agroindustrial Ltda, Carvão Ativado Industrial, 2023. https://brascarbo.com.br/. (Accessed 6 August 2021).
[15] Y. Park, D.M.Y. Kim, H.A.C. Lee, Adsorption isotherms of CO 2 , CO , N 2 , CH 4 , Ar and H 2 on activated carbon and zeolite LiX up to 1 . 0 MPa, 631–647, https://doi.org/10.1007/s10450-014-9608-x, 2014.
[16] P.C. Vilella, J.A. Lira, D.C.S. Azevedo, M. Bastos-Neto, R. Stefanutti, Preparation of biomass-based activated carbons and their evaluation for biogas upgrading purposes, Ind. Crops Prod. 109 (2017) 134–140, https://doi.org/10.1016/j.indcrop.2017.08.017.
[17] I. Durán, N. Álvarez-Gutiérrez, F. Rubiera, C. Pevida, Biogas purification by means of adsorption on pine sawdust-based activated carbon: impact of water vapor, Chem. Eng. J. 353 (2018) 197–207, https://doi.org/10.1016/j.cej.2018.07.100.
[18] F.B. Scheufele, E.S. Da Silva, B.B. Cazula, D.S. Marins, R. Sequinel, C.E. Borba, G.S. Patuzzo, T.F.M. Lopez, H.J. Alves, Mathematical modeling of low-pressure H2S adsorption by babassu biochar in fixed bed column, J. Environ. Chem. Eng. 9 (2021), https://doi.org/10.1016/j.jece.2021.105042.
[19] M. Feroldi, A.C. Neves, C.E. Borba, H.J. Alves, Methane storage in activated carbon at low pressure under different temperatures and flow rates of charge, J. Clean. Prod. 172 (2018) 921–926, https://doi.org/10.1016/j.jclepro.2017.10.247.
[20] J. Castro-Gutiérrez, N. Díez, M. Sevilla, M.T. Izquierdo, J. Ghanbaja, A. Celzard, V. Fierro, High-rate capability of supercapacitors based on tannin-derived ordered mesoporous carbons, ACS Sustain Chem Eng 7 (2019) 17627–17635, https://doi.org/10.1021/acssuschemeng.9b03407.
[21] J. Jagiello, J. Castro-Gutiérrez, R.L.S. Canevesi, A. Celzard, V. Fierro, Comprehensive analysis of hierarchical porous carbons using a dual-shape 2D-NLDFT model with an adjustable slit–cylinder pore shape boundary, ACS Appl. Mater. Interfaces 13 (2021) 49472–49481, https://doi.org/10.1021/acsami.1c13910.
[22] K. Uddin, M. Amirul Islam, S. Mitra, J. boong Lee, K. Thu, B.B. Saha, S. Koyama, Specific heat capacities of carbon-based adsorbents for adsorption heat pump application, Appl. Therm. Eng. 129 (2018) 117–126, https://doi.org/10.1016/j.applthermaleng.2017.09.057.
[23] N. Querejeta, S. García, N. Álvarez-Gutiérrez, F. Rubiera, C. Pevida, Measuring heat capacity of activated carbons for CO2 capture, J. CO2 Util. 33 (2019) 148–156, https://doi.org/10.1016/j.jcou.2019.05.018.
[24] gPROMS Process/gSW – 1145 gML: Separations – Adsorption – Isotherm Equations), No Title, 2022.
[25] I. Langmuir, The adsorption of gases on plane surfaces of glass, mica and platinum, J. Am. Chem. Soc. 40 (1918) 1361–1403, https://doi.org/10.1021/ja02242a004.
[26] T. Nitta, M. Kuro-Oka, T. Katayama, An adsorption isotherm of multi-site occupancy model for heterogeneous surface, J. Chem. Eng. Jpn. 17 (1984) 45–52, https://doi.org/10.1252/jcej.17.45.
[27] E. Khoramzadeh, M. Mofarahi, C.H. Lee, Equilibrium adsorption study of CO2 and N2 on synthesized zeolites 13X, 4A, 5A, and beta, J. Chem. Eng. Data 64 (2019) 5648–5664, https://doi.org/10.1021/acs.jced.9b00690.
[28] S. Cavenati, C. a Grande, a E. Rodrigues, Adsorption equilibrium of methane, carbon dioxide, and nitrogen on zeolite 13X at high pressures, J. Chem. Eng. Data 49 (2004) 1095–1101, https://doi.org/10.1021/je0498917.
[29] K.M. Kim, H.T. Oh, S.J. Lim, K. Ho, Y. Park, C.H. Lee, Adsorption equilibria of water vapor on zeolite 3A, zeolite 13X, and dealuminated y zeolite, J. Chem. Eng. Data 61 (2016) 1547–1554, https://doi.org/10.1021/acs.jced.5b00927.
[30] M. Thommes, K. Kaneko, A.V. Neimark, J.P. Olivier, F. Rodriguez-Reinoso, J. Rouquerol, K.S.W. Sing, Physisorption of gases, with special reference to the evaluation of surface area and pore size distribution (IUPAC Technical Report), Pure Appl. Chem. 87 (2015) 1051–1069, https://doi.org/10.1515/pac-2014-1117.
[31] R.L.S. Canevesi, K.A. Andreassen, E.A. Da Silva, C.E. Borba, C.A. Grande, Pressure swing adsorption for biogas upgrading with carbon molecular sieve, Ind. Eng. Chem. Res. 57 (2018) 8057–8067, https://doi.org/10.1021/acs.iecr.8b00996.
[32] S. Rattanaphan, T. Rungrotmongkol, P. Kongsune, Biogas improving by adsorption of CO2 on modified waste tea activated carbon, Renew. Energy 145 (2020) 622–631, https://doi.org/10.1016/j.renene.2019.05.104.
[33] H.P. Boehm, Surface oxides on carbon and their analysis: a critical assessment, Carbon N Y 40 (2002) 145–149, https://doi.org/10.1016/S0008-6223(01)00165-8.
[34] Z.H. Ho, L.A. Adnan, Phenol removal from aqueous solution by adsorption technique using coconut shell activated carbon, Tropical Aquatic and Soil Pollution 1 (2021) 98–107, https://doi.org/10.53623/tasp.v1i2.21.
[35] A.N. Módenes, F.R. Espinoza-Quiñones, C.A.Q. Geraldi, D.R. Manenti, D.E.G. Trigueros, A.P. De Oliveira, C.E. Borba, A.D. Kroumov, Assessment of the banana pseudostem as a low-cost biosorbent for the removal of reactive blue 5G dye, Environ. Technol. (2015), https://doi.org/10.1080/09593330.2015.1051591.
[36] A.I. Bakti, P.L. Gareso, Characterization of active carbon prepared from coconuts shells using FTIR, XRD and SEM techniques, Jurnal Ilmiah Pendidikan Fisika Al-Biruni. 7 (2018) 33–39, https://doi.org/10.24042/jipfalbiruni.v7i1.2459.
[37] Y. Liu, X. Liu, W. Dong, L. Zhang, Q. Kong, W. Wang, Efficient adsorption of sulfamethazine onto modified activated carbon: a plausible adsorption mechanism, Sci. Rep. 7 (2017) 1–12, https://doi.org/10.1038/s41598-017-12805-6.
[38] F. Rainone, O. D'Agostino, A. Erto, M. Balsamo, A. Lancia, Biogas upgrading by adsorption onto activated carbon and carbon molecular sieves: experimental and modelling study in binary CO2/CH4 mixture, J. Environ. Chem. Eng. 9 (2021) 106256, https://doi.org/10.1016/j.jece.2021.106256.
[39] Y. Guo, C. Tan, J. Sun, W. Li, J. Zhang, C. Zhao, Porous activated carbons derived from waste sugarcane bagasse for CO2 adsorption, Chem. Eng. J. 381 (2020) 122736, https://doi.org/10.1016/j.cej.2019.122736.
[40] R. Bai, J. Deng, R. Yang, Improved multisite Langmuir model for mixture adsorption using multiregion adsorption theory, Langmuir 19 (2003) 2776–2781, https://doi.org/10.1021/la020838v.
[41] J.M. Kolle, M. Fayaz, A. Sayari, Understanding the effect of water on CO2 adsorption, Chem. Rev. 121 (13) (2021) 7280–7345, https://doi.org/10.1021/acs.chemrev.0c00762.
[42] D.D. Do, H.D. Do, A model for water adsorption in activated carbon, Carbon 38 (2000) 767–773, https://doi.org/10.1016/S0008-6223(99)00159-1.